Fuel 179 (2016) 108–113

Contents lists available at ScienceDirect

Fuel

journal homepage: www.elsevier.com/locate/fuel

Surface functional groups and sp^3/sp^2 hybridization ratios of in-cylinder soot from a diesel engine fueled with *n*-heptane and *n*-heptane/toluene

Ye Liu [a], Chonglin Song [a,*], Gang Lv [a], Xiaofeng Cao [a], Lin Wang [a], Yuehan Qiao [b], Xinle Yang [b]

[a] State Key Laboratory of Engines, Tianjin University, Tianjin 300072, China
[b] School of Mechanical Engineering, Liaoning Technical University, Liaoning 123000, China

HIGHLIGHTS

- In-cylinder soot from *n*-heptane and *n*-heptane/toluene fueled-diesel engine was studied.
- Surface functional groups (SFGs) and sp^3/sp^2 hybridization ratios were assessed.
- Adding toluene to *n*-heptane increased the concentrations of SFGs.
- The sp^3/sp^2 hybridization ratio was obviously increased by toluene addition.
- Aliphatic C—H groups had a correlation with sp^3/sp^2 hybridization ratios.

ARTICLE INFO

Article history:
Received 23 January 2016
Received in revised form 21 March 2016
Accepted 22 March 2016
Available online 29 March 2016

Keywords:
Diesel engine
Surface functional group
sp^3/sp^2 hybridization ratio
In-cylinder soot
n-Heptane
Toluene

ABSTRACT

This work compared the surface functional group (SFG) types and concentrations and sp^3/sp^2 hybridization ratios of in-cylinder soot samples generated by a heavy-duty diesel engine when employing *n*-heptane and a toluene/*n*-heptane mixture (20% toluene by volume) as the fuels. In-cylinder soot samples were obtained from a total cylinder sampling system, and the SFGs and sp^3/sp^2 hybridization ratios were analyzed using Fourier transform infrared and X-ray photoelectron spectroscopy. Despite the differences in fuel formulation, both *n*-heptane and *n*-heptane/toluene soot exhibited similar trends in terms of changes in the SFGs concentrations and sp^3/sp^2 hybridization ratios during the combustion process. However, the addition of toluene to the *n*-heptane was found to increase the concentrations of all SFGs as well as the sp^3/sp^2 hybridization ratio. The C—OH and C═O group concentrations exhibited a bimodal distribution for both the *n*-heptane and *n*-heptane/toluene soot throughout the combustion process, with the concentrations peaking in the premixed and diffusion combustion phases, respectively. In contrast, the relative amounts of aliphatic C—H groups decreased in the premixed combustion phase, increased in the early diffusion combustion phase, and then decreased in the subsequent combustion phase. The sp^3/sp^2 hybridization ratios obtained from both fuel soot were observed to initially decrease, then to increase before a decrease during the combustion process. There was a definite correlation between the sp^3/sp^2 hybridization ratio and the relative concentration of aliphatic C—H groups.

1. Introduction

Functional groups on soot surface are produced as intermediates during soot formation and oxidation [1–5], and play an important role in both these processes. For example, the thermal decomposition of surface functional groups (SFGs) can physically and chemically reduce the barriers to lamella realignment, thus mediating the reorganization of carbon lamella [6] and altering the soot structure. During soot oxidation, C—H and oxygenated functional groups attached to non-six-membered carbon rings behave as highly reactive edges, providing a greater number of the reactive sites for the facile oxidation of soot [7–11]. Moreover, sp^3 and sp^2 hybridizations are the main chemical states of carbon in soot, and the amounts and spatial relationships of the carbon atoms in these two states are intimately linked to soot formation [12]. Thus, it is important to gain insights into the SFGs and sp^3/sp^2 hybridization ratio of soot to understand the soot formation and oxidation mechanisms.

Within the combustion history, the initial fuel composition plays a key role in the types and concentrations of SFGs and sp^3/sp^2 hybridization ratio of soot. Alfè et al. [13] reported that

* Corresponding author. Tel.: +86 22 27406840x8020; fax: +86 22 27403750.
E-mail address: songchonglin@tju.edu.cn (C. Song).

http://dx.doi.org/10.1016/j.fuel.2016.03.082
0016-2361/

the soot produced from benzene and cyclohexane premixed flames contained relatively fewer C—H SFGs compared with the soot obtained from methane and ethylene premixed flames, and thus concluded that the amount of C—H groups on the soot surface was dependent upon the fuel nature. After examining the soot generating from several emission sources, Vander Wal et al. [12] found that the fuel oxygen content had a marked effect on the sp^2/sp^3 hybridization ratio. In the case of diesel-generated soot, it is very difficult to determine the impact of fuel composition on the SFGs and sp^3/sp^2 hybridization ratios because of the component complexity of conventional diesel fuel. For this reason, the alkane hydrocarbon *n*-heptane, which has a cetane number close to that of diesel fuel and for which the oxidation chemistry is very well known, has been widely employed as a surrogate for hydrocarbon fuels in diesel engines [14,15]. Aromatics account for a large fraction of conventional diesel fuels (about 25–35% by weight on average) [16,17] and toluene is representative of many of these aromatic compounds [18]. Thus, the *n*-heptane/toluene mixture has been proposed as a more suitable surrogate for the alkanes and aromatics in diesel fuel in experimental and numerical studies [15,19].

To date, the studies on the SFG and sp^3/sp^2 hybridization ratio have focused almost exclusively on the soot generated from laboratory flames [20–22] or diesel exhausts [8–11,23]. Due to the high pressure and temperature environment for the diesel combustion, there have been few reports on the SFGs and sp^3/sp^2 hybridization ratio of diesel in-cylinder soot. The properties of SFGs and sp^3/sp^2 hybridization ratio for the soot generated from laboratory flame differ substantially from those for the diesel in-cylinder soot due to differences in combustion processes, combustion temperature and gas pressure, all of which play an important role in the formation and decomposition of SFGs and the sp^3/sp^2 hybridization ratio [8,12]. Furthermore, the information obtained from exhaust soot can only provide the features of the SFGs and sp^3/sp^2 hybridization ratio of the mature diesel soot. In this context, this paper provided comprehensive characterization of the SFGs and sp^3/sp^2 hybridization ratio of diesel in-cylinder soot when *n*-heptane and an *n*-heptane/toluene mixture as fuels were burned in a diesel engine. A total cylinder sampling system was employed to obtain the in-cylinder soot samples. The aliphatic C—H functional groups on the obtained in-cylinder soot surface were measured using Fourier transform infrared (FT-IR) spectroscopy, while the oxygenated functional groups and sp^3/sp^2 hybridization ratios were assessed by X-ray photoelectron spectroscopy (XPS). In addition, an attempt was made to obtain a correlation between the SFGs and the sp^3/sp^2 hybridization ratios.

2. Materials and methods

A 5.79 L heavy-duty, direct-injection diesel engine was used in this study. This engine was equipped with a high-pressure, common-rail fuel injection system and a turbocharged/intercooled air intake system and powered up to 132 kW at a maximum speed of 2600 rpm. The sixth cylinder was modified as a total cylinder sampling system to allow the sampling of soot directly from the combustion chamber. During sampling, an aluminum alloy diaphragm was used to seal the engine cylinder head, acting as a sampling valve. At a pre-set crank angle during a sampling cycle, this diaphragm was instantaneously cut by an electromagnet-actuated tube cutter, following which the cylinder contents were discharged from the cylinder into a sampling bag. The samples were immediately quenched and diluted by mixing with high pressure nitrogen to obtain a temperature below 52 °C, to prevent any additional reactions during the sampling process. A detailed description of this apparatus and sampling procedure has previously been reported in the literature [17,24–26].

The engine operating conditions are provided in Table 1. Two diesel fuel surrogates were used: *n*-heptane and a mixture of 80 vol.% *n*-heptane and 20 vol.% toluene (termed *n*-heptane/toluene). The relevant properties of both fuels have been described in the literature [25]. Different injection time intervals were employed to ensure the same equivalence ratios for the *n*-heptane and *n*-heptane/toluene fuels. Because the content of toluene in the *n*-heptane/toluene mixture was only 20%, the ignition delay when using the *n*-heptane/toluene was almost the same as when using the *n*-heptane fuel at the same equivalence ratio. Both fuels exhibited almost the same behavior in terms of the apparent heat release rates, in-cylinder pressures and average temperatures (see Fig. 1). To characterize the in-cylinder soot during combustion process, five representative sampling points were chose to represent the different diesel combustion phases according to the plots of in-cylinder pressure and apparent heat release rate in Fig. 1. The determination of the diesel combustion phase followed the method suggested by Heywood [27]: in the premixed combustion phase, the heat release rate is generally very high and the period corresponds to the rapid cylinder pressure rise. The dif-

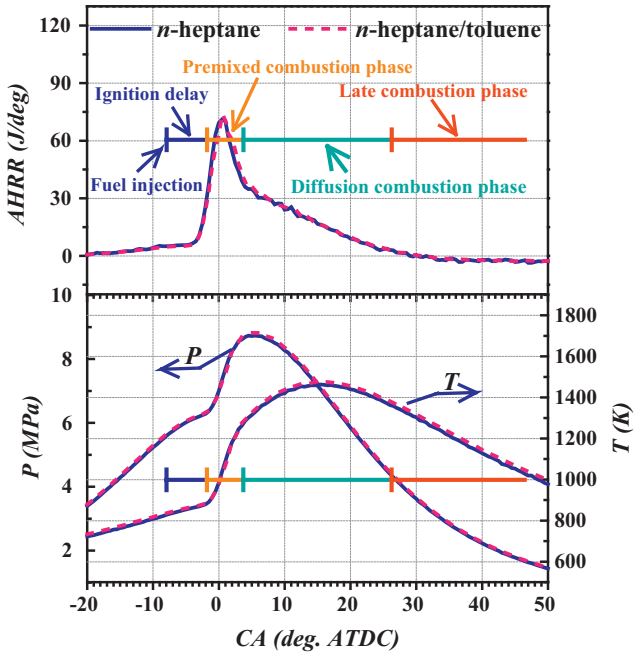

Fig. 1. Cylinder gas pressure (*P*), mean temperature (*T*) and apparent heat release rate (AHRR) as functions of crank angle (CA), identifying different diesel combustion phases.

Table 1
Diesel engine operating conditions.

Fuel	Engine speed (rpm)	Common rail pressure (MPa)	Start of injection (°CA ATDC)	Duration of injection (ms)	Fuel–air equivalence ratio (Φ)	Intake temperature (K)
n-Heptane	1000	60	−8	0.800	0.267	318
n-Heptane/toluene	1000	60	−8	0.832	0.264	318

fusion combustion phase corresponds to a period of gradually decreasing heat release rate. In the late combustion phase, the heat release rate usually amounts to about 20% of the total fuel energy. The five sampling points used corresponded to the onset of the premixed combustion phase, the late premixed combustion phase, the early diffusion combustion phase, the middle of the diffusion combustion phase and the late combustion phase. Because only small amounts of soot were generated in each combustion cycle, the sampling procedure was repeated at least five times at the same pre-set sampling crank angle. Samples were collected on Teflon filters (R2PL047; PallGelman, USA), and the soot was removed by ultrasonication in dichloromethane, followed by centrifugal separation [17]. The resulting soot samples were dried under nitrogen and then sealed in glass bottles while awaiting analysis. Owing to the heterogeneous nature of diesel combustion, each total cylinder sample could potentially contain a mixture of young and mature soot at various stages of formation and growth. Therefore, the data obtained essentially represented the statistically averaged properties of the soot.

FT-IR spectroscopy was employed to identify the functional groups and to quantify the relative amounts of aliphatic C—H groups on the soot surface. A Nicolet Nexus 470 FT-IR spectrometer with a resolution of 1 cm^{-1} was used with the KBr tablets. The KBr tablets were prepared by mixing and grinding the soot in KBr pellets (0.5 wt%) and the mixed-dispersions were compressed at 10 Ton for 5 min into a thin disk. Spectra were baseline-corrected and smoothed prior to analysis. A continuous background was subtracted from the sample spectra in the baseline correction procedure. The absorbance spectra were generated using the OMNIC software package (Thermo Nicolet). Three spectra were acquired for each sample to ensure reproducibility, and the variations in the FT-IR measurements were found to be less than 5%.

Information on the oxygenated functional group, the O/C elemental ratio and the carbon chemical state in the soot samples was obtained by X-ray photoelectron spectroscopy (XPS). XPS spectra were recorded on a PerkinElmer PHI-1600 ESCA spectrometer using a Mg Kα X-ray source. The binding energies were calibrated using the C 1s peak of contaminant carbon (BE = 284.6 eV) as an internal standard. The XPS results from three different sections of each soot sample were averaged, and an uncertainty of less than 6% was attained.

3. Results and discussion

3.1. Aliphatic C—H SFGs

FT-IR spectroscopy was employed to investigate the aliphatic C—H SFGs of the *n*-heptane and *n*-heptane/toluene soot. Fig. 2 shows a typical baseline-corrected, smoothed FT-IR spectrum obtained from an in-cylinder *n*-heptane sample. According to Mckinnon et al. [28], Stantamaría et al. [29] and our own previous work [17], the ratio of the aliphatic C—H peak at 2925 cm^{-1} to the aromatic C=C peak at 1620 cm^{-1} (I_{2925}/I_{1620}) can be used to determine the relative concentrations of aliphatic C—H groups. Fig. 3 plots the I_{2925}/I_{1620} values as functions of crank angle (CA). The I_{2925}/I_{1620} values for the *n*-heptane/toluene soot were evidently larger than those for the *n*-heptane soot at the same combustion stage. Aliphatic C—H groups primarily stem from methyl, methylene, and methane groups bonded to aromatic rings on polycyclic aromatic hydrocarbons (PAHs) or the methylene bridges (fluorine type) maintaining the interconnection of PAHs within a network [28,29]. According to the studies of Vander Wal and his colleagues [30–32], the incorporation of odd-number rings within the carbon plane accounts for curvature in lamella, which can give rise to disorder within the carbon framework by preventing development of

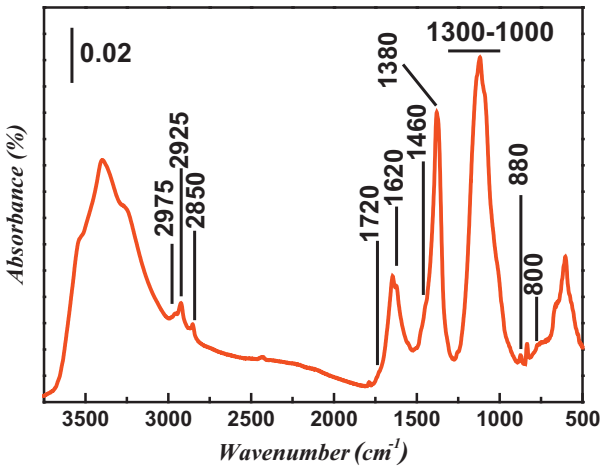

Fig. 2. Typical FT-IR spectrum of an in-cylinder *n*-heptane soot sample (−1.5° CA ATDC).

stacked layers. Al-Qurashi et al. [33] also found that the existence of wave structure (or tortuosity) in the layer plane may be attributed to lattice defect and/or the existence of odd-number ring structures. The *n*-heptane/toluene soot has a more highly curved nanostructure than the *n*-heptane soot because the addition of toluene is known to enhance the generation of PAHs containing five-membered rings [30,34,35]. This highly curved nanostructure can provide more active sites for the binding of aliphatics [9,10,21,36], leading to an increase in the number of aliphatic C—H groups on the soot surface.

During the same combustion stage, the *n*-heptane and *n*-heptane/toluene soot shows almost the same trend in the I_{2925}/I_{1620} ratios with increasing CA. In our previous study [17], the conventional diesel soot also exhibited similar trend in terms of changes in I_{2925}/I_{1620} ratio throughout the combustion process. This phenomenon appears to show that during the combustion of diesel engines the trend in terms of changes in aliphatic C—H groups on soot surface depends on combustion condition rather than on the fuel composition. Moreover, in the initial premixed combustion phase, the higher I_{2925}/I_{1620} values observed for both the *n*-heptane and *n*-heptane/toluene soot indicate that a greater number of aliphatic C—H groups were bonded to the soot surface. The high aliphatic C—H group concentrations on the soot surface can likely be attributed to the presence of many young soot particles with aliphatic shells in the initial combustion stage [22,29]. As

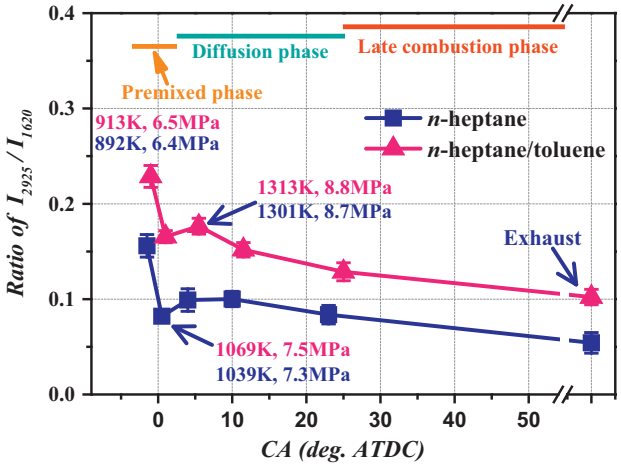

Fig. 3. I_{2925}/I_{1620} ratios as functions of crank angle (CA). The error bars represent the standard error.

the combustion proceeded, both types of soot underwent decreases in the I_{2925}/I_{1620} ratio because the increased cylinder pressure and mean temperature enhanced the dehydrogenation and carbonization reactions of the soot, and thus lowered the aliphatic C—H amounts on the soot surface. In the early diffusion combustion phase, the slight increases in the I_{2925}/I_{1620} values were mainly caused by the presence of large quantities of young soot particles generated in this phase. During the subsequent combustion phases, dehydrogenation and carbonization reaction resulted in the persistent decrease in the value of I_{2925}/I_{1620}.

3.2. Oxygenated functional groups and O/C

XPS analyses were performed to obtain information about the oxygenated functional groups and the compositions of the soot surface. Fig. 4 shows a high-resolution scan of the typical C 1s peaks of the *n*-heptane soot. To allow for quantitative analysis, the C 1s region was deconvolved, and the resulting fitted peaks at 286.6 and 288.4 eV were assigned to hydroxyl (C—OH) and carbonyl (C=O) groups, respectively [12,23]. The concentrations of C—OH and C=O groups found in the *n*-heptane/toluene and *n*-heptane soot are plotted against CA in Fig. 5. Here, it is evident that the amounts of both groups are higher in the *n*-heptane/toluene soot at the same combustion stage. Both C=O and C—OH groups are generated as intermediates upon partial oxidation of soot by OH, O and other radicals [11], and the types and concentrations of the resulting SFGs depend primarily on the fuel composition [12,13]. Because the *n*-heptane/toluene soot had a highly curved nanostructure, as noted above, it was able to furnish more active sites for the bonding of OH and O radicals during soot oxidation, generating more C—OH and C=O groups on the soot surface.

Similar to the results shown in Fig. 3, the trends in terms of changes in the concentrations of the C—OH and C=O groups were alike for both *n*-heptane and *n*-heptane/toluene throughout the combustion process (Fig. 5). In the premixed combustion phase, the increased cylinder pressure and temperature promoted the partial oxidation of the soot, resulting in increased concentrations of C—OH and C=O groups as intermediates in both *n*-heptane and *n*-heptane/toluene soot. As the combustion proceeded from the late premixed stage to the early diffusion stage, both *n*-heptane and *n*-heptane/toluene soot showed a decrease in the concentrations of both oxygenated functional groups, likely due to the presence of young soot particles with few oxygenated

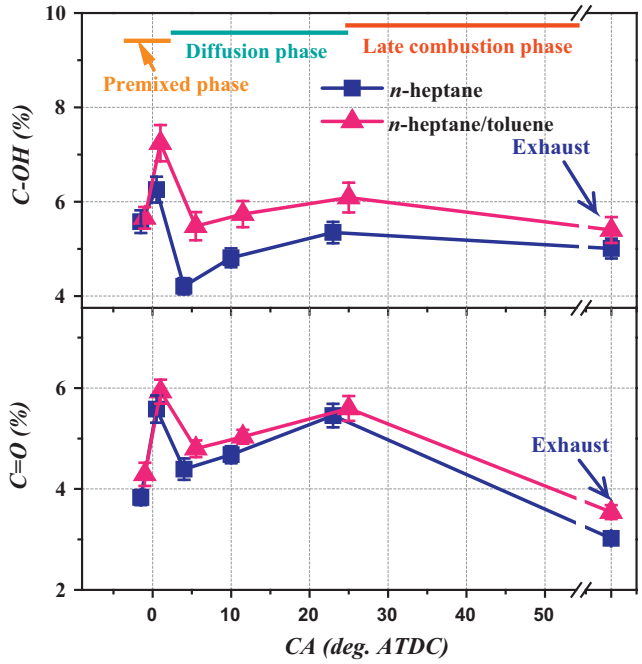

Fig. 5. Concentrations of C—OH and C=O surface functional groups as functions of crank angle (CA). The error bars indicate the standard error.

SFGs that were generated in this phase [21]. Subsequently, the soot was partially oxidized in the late diffusion combustion phase, and more C—OH and C=O groups were generated on the soot surface. Finally, in the late combustion phase, the decreased concentrations of C—OH and C=O groups are believed to be related to a reduction in soot oxidation associated with the lower cylinder pressure and temperature.

The ratios of O to C atoms (O/C) on the soot surface were obtained from the areas of the O 1s and C 1s peaks in the XPS spectra, and Fig. 6 plots the O/C ratios for the *n*-heptane and *n*-heptane/toluene soot as functions of CA. During the same combustion phase, the ratio obtained from the *n*-heptane/toluene soot is larger than that from the *n*-heptane soot. This is not surprising because the majority of the O atoms detected using this method are present in oxygenated groups bonded to the soot surface [37], and the *n*-heptane/toluene soot had a higher concentration of oxygenated

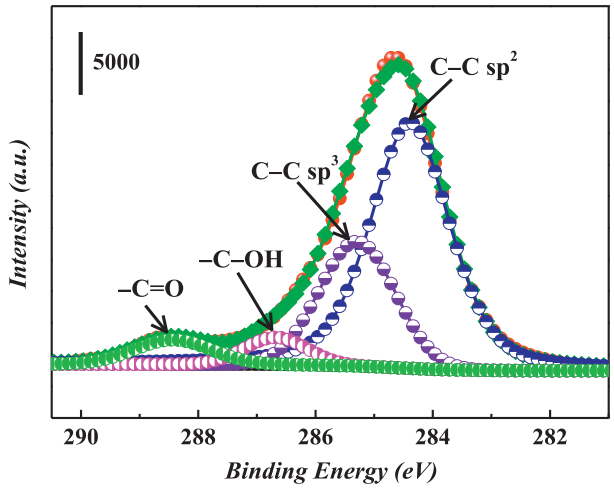

Fig. 4. Typical XPS C 1s narrow spectra for an *n*-heptane soot sample (−1.5° CA ATDC). (C=O: ◐, C—OH: ◑, C—C sp^2: ◓, C—C sp^3: ◒, fit curve: ◆ and original C 1s curve: ●).

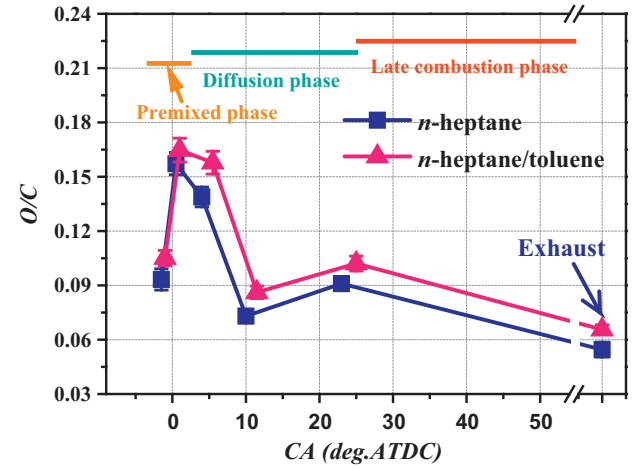

Fig. 6. O/C atomic ratios as functions of crank angle (CA). The error bars indicate the standard error.

groups relative to the *n*-heptane soot. The O/C ratios varied over the ranges of 0.05–0.16 for the *n*-heptane soot and 0.07–0.17 for the *n*-heptane/toluene soot over the entire combustion period. In the case of diesel fuel in-cylinder soot, the ratio is typically in the range of 0.08–0.14 [17]. These results therefore indicate that the fuel composition has only a marginal effect on the O/C ratio in diesel engine in-cylinder soot.

3.3. Ratio of sp^3/sp^2 hybridization

The XPS spectra for the main carbon peak can be resolved by deconvolution into two peaks, as illustrated in Fig. 4. The main peak, at approximately 284.3 eV, corresponds to sp^2 hybridized 2D carbon (graphite), which represents ordered carbon [3], while the peak centered near 285.4 eV is attributed to sp^3 hybridized 3D carbon (diamond) [38,39]. The sp^3 hybridized carbon atoms represent defects that can disrupt the sp^2 hybridized network and require bond terminations other than adjacent π bonded carbon atoms. These atoms decrease the long-range order and accordingly are considered to represent defect sites [12]. Therefore, a large sp^3/sp^2 hybridization ratio indicates a more highly amorphous structure [13,40]. Fig. 7 plots the sp^3/sp^2 hybridization ratios as functions of CA for both *n*-heptane and *n*-heptane/toluene soot samples. The ratio values of the *n*-heptane/toluene soot are higher than those of the *n*-heptane soot in each combustion phase, demonstrating that the *n*-heptane/toluene soot had a more disordered, amorphous structure than the *n*-heptane soot. Similar data have been reported by Vander Wal et al. [41], who found that benzene soot presented a more amorphous structure as compared with acetylene soot in a premixed flame. Jaramillo et al. [42] also observed that *m*-xylene/*n*-dodecane soot had a higher sp^3/sp^2 hybridization ratio than *n*-dodecane soot in a premixed flat flame.

Interestingly, the trends in terms of changes in the sp^3/sp^2 hybridization ratio in Fig. 7 are similar for both the *n*-heptane/toluene and *n*-heptane soot throughout the entire combustion process, indicating that the ratio is independent of the fuel composition. During the premixed combustion phase, there was a dramatic decrease in the ratio for both the *n*-heptane and *n*-heptane/toluene soot, implying an increase in graphitic planar structures within the soot. Between the late premixed combustion and the early diffusion combustion phases, the disordered structure of the soot increased, as shown by the slightly increased sp^3/sp^2 hybridization ratios. This is ascribed to the presence of a great number of newly generated soot particles with amorphous structure [24,25]. As the combustion proceeded to the late diffusion phase, the rapidly increased cylinder pressure and temperature enhanced the graphitic structure of these newly formed soot particles, and thus the sp^3/sp^2 hybridization ratios decreased for both soot samples. In the late combustion phase, the evolution of graphitic structure was lessened by the steep reductions in the cylinder pressure and temperature. However, at the same time, the soot particles generated possessed more defined graphitic structures and hence had higher resistance to further graphitization. Consequently, the sp^3/sp^2 hybridization ratios slightly decreased in this phase.

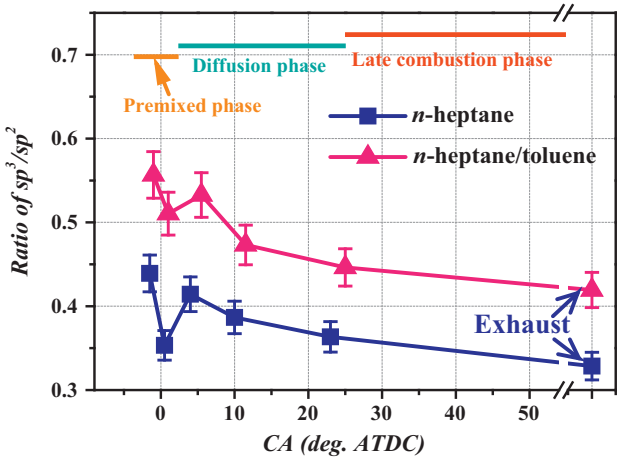

Fig. 7. sp^3/sp^2 hybridization ratios as functions of crank angle (CA). The error bars indicate the standard error.

3.4. Relationship between SFG and sp^3/sp^2 hybridization ratio

To establish a possible correlation, the measured SFG concentrations and sp^3/sp^2 hybridization ratios were plotted, as shown in Fig. 8. Although the data in this figure were obtained from the *n*-heptane and *n*-heptane/toluene soot at various combustion stages, the soot samples with larger I_{2925}/I_{1620} ratios generally show higher sp^3/sp^2 hybridization ratios as well, implying that the presence of aliphatic C—H groups is definitely correlated with the hybridization ratio. The extent of correlation between I_{2925}/I_{1620} values and the sp^3/sp^2 hybridization ratios was assessed based on the linear correlation coefficient, R^2, which was obtained by means of simple linear regression. The R^2 values for the *n*-heptane and *n*-heptane/toluene soot were 0.83 and 0.90, respectively. In contrast, the oxygenated SFGs did not show any correlation with the sp^3/sp^2 hybridization ratio; plots of C—OH or C=O concentrations as functions of the sp^3/sp^2 ratio showed a scattered distribution. These results demonstrate that the relative amounts of aliphatic C—H groups can serve as an indicator of the sp^3/sp^2 hybridization ratio in soot. This conclusion is consistent with the findings of Alfè et al. [13], who reported that a decrease in the

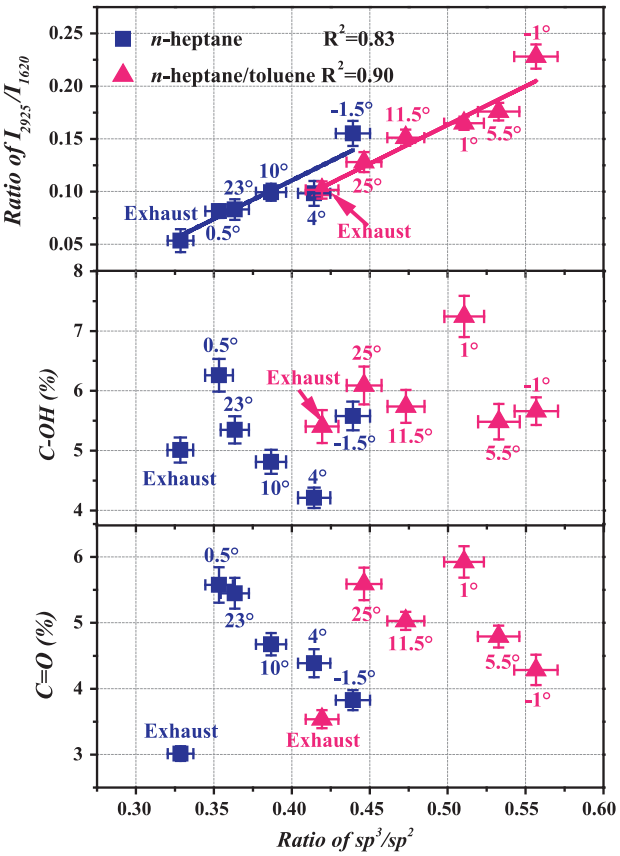

Fig. 8. I_{2925}/I_{1620} ratios and concentrations of C—OH and C=O as functions of the sp^3/sp^2 ratio. The error bars indicate the standard error.

aliphatic groups in premixed flame soot coincides with a decrease in the sp^3/sp^2 hybridization ratio.

4. Conclusion

A comparative study of SFGs and sp^3/sp^2 hybridization ratios in in-cylinder soot samples was performed, employing a heavy-duty diesel engine fueled with *n*-heptane and *n*-heptane/toluene. Despite the different fuel formulation employed, the trends in terms of changes in I_{2925}/I_{1620} ratios, concentrations of both C—OH and C=O groups and sp^3/sp^2 hybridization ratios for *n*-heptane were similar to those for *n*-heptane/toluene soot over the combustion process. However, the *n*-heptane/toluene soot exhibited relatively high concentrations of aliphatic C—H, C—OH and C=O groups as well as greater sp^3/sp^2 hybridization ratios with respect to the *n*-heptane soot throughout the combustion process. The I_{2925}/I_{1620} ratios determined for both soot samples showed an increase in the early diffusion phase after a sharp decrease in the premixed combustion phase, as well as a gradual decline in the subsequent combustion phase. Under the engine operating condition applied, the concentrations of C—OH and C=O groups in the *n*-heptane/toluene soot were found to be in the range of 4.81–6.26% and 3.02–5.58%, respectively, while the *n*-heptane soot had levels ranging from 5.40–7.24% and 3.54–5.93%, respectively. In the case of both the *n*-heptane and *n*-heptane/toluene soot samples, the sp^3/sp^2 hybridization ratios presented a similar trend to the I_{2925}/I_{1620} ratios throughout the combustion phase. Finally, the relative amounts of aliphatic C—H SFGs exhibited a clear correlation with the sp^3/sp^2 hybridization ratio, while no such correlation was found with the oxygenated SFGs.

Acknowledgments

This study was supported by the National Natural Science Foundation of China (No. 51476115) and the National Key Basic Research and Development Program (No. 2013CB228502), and the Tianjin Research Program of Application Foundation and Advanced Technology (13JCZDJC35800).

References

[1] Held TJ, Marchese AJ, Dryer FL. A semi-empirical reaction mechanism for *n*-heptane oxidation and pyrolysis. Combust Sci Technol 1997;123:107–46.
[2] Curran H, Gaffuri P, Pitz WJ, Westbrook CK. A comprehensive modeling study of *n*-heptane oxidation. Combust Flame 1998;114:149–77.
[3] Agafonov GL, Naydenova I, Vlasov PA, Warnatz J. Detailed kinetic modeling of soot formation in shock tube pyrolysis and oxidation of toluene and *n*-heptane. Proc Combust Inst 2007;31:575–83.
[4] Blanquart G, Pepiot-Desjardins P, Pitsch H. Chemical mechanism for high temperature combustion of engine relevant fuels with emphasis on soot precursors. Combust Flame 2009;156:588–607.
[5] Santamaría A, Eddings EG, Mondragón F. Effect of ethanol on the chemical structure of the soot extractable material of an ethylene inverse diffusion flame. Combust Flame 2007;151:235–44.
[6] Vander Wal RL, Yezerets A, Currier NW, Kim DH, Wang CM. HRTEM study of diesel soot collected from diesel particulate filters. Carbon 2007;45:70–7.
[7] Su DS, Jentoft RE, Müller JO, Rothe D, Jacob E, Simpson CD, et al. Microstructure and oxidation behaviour of Euro IV diesel engine soot: a comparative study with synthetic model soot substances. Catal Today 2004;90:127–32.
[8] Song J, Alam M, Boehman AL, Kim U. Examination of the oxidation behavior of biodiesel soot. Combust Flame 2006;146:589–604.
[9] Al-Qurashi K, Lueking AD, Boehman AL. The deconvolution of the thermal, dilution, and chemical effects of exhaust gas recirculation (EGR) on the reactivity of engine and flame soot. Combust Flame 2011;158:1696–704.
[10] Edwards IA, Menendez R, Marsh H. Introduction to carbon science. London: Butterworth-Heinemann; 1989. p. 107–52.
[11] Williams S. Surface intermediates, mechanism, and reactivity of soot oxidation, Ph.D. thesis, University of Toronto, Toronto, 2008.
[12] Vander Wal RL, Bryg VM, Hays MD. XPS analysis of combustion aerosols for chemical composition, surface chemistry, and carbon chemical state. Anal Chem 2011;83:1924–30.
[13] Alfè M, Apicella B, Barbella R, Rouzaud J-N, Tregrossi A, Ciajolo A. Structure–property relationship in nanostructures of young and mature soot in premixed flames. Proc Combust Inst 2009;32:697–704.
[14] D'Anna A, Alfè M, Apicella B, Tregrossi A, Ciajolo A. Effect of fuel/air ratio and aromaticity on sooting behavior of premixed heptane flames. Energy Fuel 2007;21:2655–62.
[15] Luo J, Yao M, Liu H, Yang B. Experimental and numerical study on suitable diesel fuel surrogates in low temperature combustion conditions. Fuel 2012;97:621–9.
[16] Sharma A, Kyotani T, Tomita A. Comparison of structural parameters of PF carbon from XRD and HRTEM techniques. Carbon 2000;38:1977–84.
[17] Wang L, Song CL, Song JO, Lv G, Pang HT, Zhang W. Aliphatic C–H and oxygenated surface functional groups of diesel in-cylinder soot: characterizations and impact on soot oxidation behavior. Proc Combust Inst 2013;34:3099–106.
[18] Hellier P, Ladommatos N, Allan R, Rogerson J. Combustion and emissions characteristics of toluene/*n*-heptane and 1-octene/*n*-octane binary mixtures in a direct injection compression ignition engine. Combust Flame 2013;160:2141–58.
[19] Andrae J, Johansson D, Björnbom P, Risberg P, Kalghatgi G. Co-oxidation in the auto-ignition of primary reference fuels and *n*-heptane/toluene blends. Combust Flame 2005;140:267–86.
[20] Santamaría A, Mondragón F, Molina A, Marsh ND, Eddings EG, Sarofim AF. FT-IR and ^{1}H NMR characterization of the products of an ethylene inverse diffusion flame. Combust Flame 2006;146:52–62.
[21] Cain JP, Camacho J, Phares DJ, Wang H, Laskin A. Evidence of aliphatics in nascent soot particles in premixed ethylene flames. Proc Combus Inst 2011;33:533–40.
[22] Wang H. Formation of nascent soot and other condensed-phase materials in flames. Proc Combust Inst 2011;33:41–67.
[23] Vander Wal RL, Bryg VM, Hays MD. Fingerprinting soot (towards source identification): physical structure and chemical composition. J Aerosol Sci 2010;41:108–17.
[24] Li Z, Song CL, Song JO, Lv G, Dong SR, Zhao Z. Evolution of the nanostructure, fractal dimension and size of in-cylinder soot during diesel combustion process. Combust Flame 2011;158:1624–30.
[25] Wei JJ, Song CL, Song JO, Lv G, Wang L, Pang HT. A comparative study of the physical properties of in-cylinder soot generated from the combustion of *n*-heptane and toluene/*n*-heptane in a diesel engine. Proc Combust Inst 2015;35:1939–46.
[26] Wang XW, Song CL, Lv G, Song JO, Li H, Li B. Evolution of in-cylinder polycyclic aromatic hydrocarbons in a diesel engine fueled with *n*-heptane and *n*-heptane/toluene. Fuel 2015;158:322–9.
[27] Heywood JB. Internal combustion engine fundamentals. New York: McGraw Hill; 1988. p. 503–7.
[28] Mckinnon JT, Meyer E, Howard JB. Infrared analysis of flame-generated PAH samples. Combust Flame 1996;105:161–6.
[29] Santamaría A, Mondragón F, Quinonez W, Eddings EG, Sarofim AF. Average structural analysis of the extractable material of young soot gathered in an ethylene inverse diffusion flame. Fuel 2007;86:1908–17.
[30] Vander Wal RL, Tomasek AJ. Soot nanostructure: dependence upon synthesis conditions. Combust Flame 2004;136:129–40.
[31] Vander Wal RL, Tomasek AJ, Pamphlet MI, Taylor CD, Thompson WK. Analysis of HRTEM images for carbon nanostructure quantification. J Nanopart Res 2004;6:555–68.
[32] Vander Wal RL, Mueller CJ. Initial investigation of effects of fuel oxygenation on nanostructure of soot from a direct-injection diesel engine. Energy Fuel 2006;20:2364–9.
[33] Al-Qurashi K, Boehman AL. Impact of exhaust gas recirculation (EGR) on the oxidative reactivity of diesel engine soot. Combust Flame 2008;155:675–95.
[34] Yuan W, Li Y, Dagaut P, Yang J, Qi F. Experimental and kinetic modeling study of styrene combustion. Combust Flame 2015;162:1868–83.
[35] Vander Wal RL, Bryg VM, Huang C-H. Insights into the combustion chemistry within a gas-turbine driven auxiliary power unit as a function of fuel type and power level using soot nanostructure as a tracer. Fuel 2014;115:282–7.
[36] Vander Wal RL, Strzelec A, Toops TJ, Daw CS, Genzale CL. Forensics of soot: C5-related nanostructure as a diagnostic of in-cylinder chemistry. Fuel 2013;113:522–6.
[37] Dames E, Sirjean B, Wang H. Weakly bound carbon–carbon bonds in acenaphthene derivatives and hexaphenylethane. J Phys Chem A 2009;114:1161–8.
[38] Russo C, Stanzione F, Tregrossi A, Ciajolo A. Infrared spectroscopy of some carbon-based materials relevant in combustion: qualitative and quantitative analysis of hydrogen. Carbon 2014;74:127–38.
[39] Russo C, Tregrossi A, Ciajolo A. Dehydrogenation and growth of soot in premixed flames. Proc Combust Inst 2015;35:1803–9.
[40] Russo C, Alfè M, Rouzaud J-N, Stanzione F, Tregrossi A, Ciajolo A. Probing structures of soot formed in premixed flames of methane, ethylene and benzene. Proc Combust Inst 2013;34:1885–92.
[41] Vander Wal RL, Tomasek AJ. Soot oxidation: dependence upon initial nanostructure. Combust Flame 2003;134:1–9.
[42] Jaramillo IC, Gaddam CK, Vander Wal RL, Huang C-H, Levinthal JD, Lighty JS. Soot oxidation kinetics under pressurized conditions. Combust Flame 2014;161:2951–65.